A Barrier-Terrain Methodology for Global Optimization

Angelo Lucia* and Rajeswar R. Gattupalli

Department of Chemical Engineering, University of Rhode Island, Kingston, Rhode Island 02881-0805

Kedar Kulkarni and Andreas Linninger

Department of Chemical Engineering & Bioengineering, University of Illinois−Chicago, Chicago, Illinois 60607-7000

It is shown that all stationary and singular points to optimization problems do not necessarily lie in the same valley and are not necessarily smoothly connected. Logarithmic barrier functions are shown to be an effective means of finding smooth connections between distinct valleys, so that the terrain method is guaranteed to explore the entire feasible region. After valleys are connected, different stationary and singular points in separate parts of the feasible region can be calculated and identified and sequentially tracked as the barrier parameter is reduced. The proposed barrier-terrain methodology is used to successfully find all physically meaningful solutions to a small illustrative problem and a collocation model for a spherical catalyst pellet problem with 20 variables. The key contribution of this work is the discovery that barrier methods provide connections between valleys that contain stationary points for intermediate barrier parameter values under mild conditions on the model equations.

1. Introduction

Many important models of chemical engineering applications have multiple solutions that are sometimes difficult to find in the absence of prior knowledge. Examples include equations of state such as the Statistical Associating Fluid Theory (SAFT) equations, phase stability/equilibrium problems, and problems in chemical kinetics. One way to find multiple solutions is to formulate the underlying problem in the form of a global mathematical program and use a global optimization methodology such as an interval method,[1] continuation method,[2] a branch-and-bound algorithm,[3] simulated annealing,[4] genetic algorithms,[5] a terrain-following method, or some other strategy. In this article, we use the terrain method of Lucia and co-workers.[6,7]

Barrier methods of nonlinear programming are old techniques that were developed in the 1950s and are similar to penalty function methods.[8,9] In particular, logarithmic-barrier methods form the backbone of an entire class of methods called interior-point methods. The main objective of logarithmic barrier methods is to enforce feasibility on iterates in equation-solving methods such as quasi-Newton and Newton methods. Barrier methods force iterates to lie in the interior of the feasible region by constructing a function that approaches infinity at the boundaries of the feasible region. The typical functional form of a logarithmic barrier function for the simple bound $x \geq 0$ is $-\mu \log(x)$, where μ is called a barrier parameter. Barrier functions can also be used with upper bounds on variables and general inequality constraints in a straightforward manner. The key aspects of any barrier approach are as follows:

(1) To create an augmented objective function that consists of the given objective function and the barrier function.

(2) To start with a large value of the barrier parameter so that the augmented objective function is convex and has a unique minimum.

(3) To reduce the value of the barrier parameter and use a solution from the previous barrier sub-problem, $x^*(\mu_k)$, to find a solution to the current barrier sub-problem, $x^*(\mu_{k+1})$.

(4) To terminate the optimization calculations when μ is sufficiently close to zero, where the values of the augmented objective function and given objective function coincide.

Note that the barrier function ensures that iterates are always in the interior of the feasible region and the barrier parameter serves as a continuation parameter.

Barrier methods are powerful techniques; however, they are not without disadvantages. In particular, if there are *active* inequality constraints at the solution for $\mu \approx 0$, then it is well-known that the Hessian matrix of the augmented objective function becomes increasingly ill-conditioned and this ill-conditioning cannot be avoided. (See, for example, the work of Luenberger.[10]) If no inequalities are active at the solution, then the eigen-structure of the Hessian matrix at the desired solution is that of the given objective function.

In this article, we discover that barrier functions can be an effective tool to identify all solutions for global optimization with terrain methods in cases where some solutions belong to separate disconnected regions in the feasible space. To the best of our knowledge, this use of barrier functions beyond their classical purpose is reported for the first time in the open literature.

This manuscript begins with an example that shows that all stationary and singular points to optimization problems are not necessarily required to lie in the same valley and that valleys of the objective function surface are not necessarily required to be (smoothly) connected. For very large values of the barrier parameter, there is a unique solution and a single valley that leads to the boundary. Moreover, if the given problem has multiple stationary points and disconnected valleys, then the valleys will be disconnected at small values of the barrier parameter. However, somewhere between, for intermediate values of the barrier parameter, one might expect multiple stationary and singular points to be present and for the valleys to be connected. *The key result of this research clearly shows exactly this: logarithmic barrier functions can be used to create a smooth connection between stationary and singular points in distinct valleys for some set of intermediate values of the barrier parameter (μ) that are bounded away from zero so that the*

* To whom correspondence should be addressed. Tel.: 401-874-2814. E-mail address: lucia@egr.uri.edu.

10.1021/ie071421t CCC: $40.75
Published on Web 03/14/2008

terrain method is guaranteed to explore more of the feasible region. This fundamental property of barrier methods, which provides a connection between valleys that contain important stationary and singular points for some set of intermediate values of μ, is the key observation on which this research is based and, to our knowledge, has never been studied previously. After the valleys are connected at intermediate values of the barrier parameter, it is possible to identify different solutions in different basins of attraction in the feasible region and track those stationary and singular points. Distinct solution sets that belong to gradually disconnected regions serve as independent starting points as the barrier parameter is further reduced. A straightforward barrier-terrain algorithm is presented and details for a small example are presented to elucidate the underlying ideas. This is followed by the application of the proposed barrier-terrain methodology to a collocation model for a spherical catalyst pellet problem with 20 variables with a solution multiplicity of 3. Here, it is shown that the barrier-terrain method can successfully find all solutions, because it creates a smooth valley that connects all physically meaningful solutions at some values of the barrier parameter bounded well away from zero, where no natural connection exists.

One can view the barrier-terrain approach as a method that "deforms" the objective function surface. Other optimization methods have been proposed for deforming the objective function surface to find desired points. For example, Piela et al.[11] proposed a method called the diffusion equation method that finds global minima on an objective function. The diffusion equation method uses the operator $T(t) = \exp(t\, d^2/dx^2)$ and applies $T(t)$ to the objective function to deform the landscape in a way that eliminates shallow minima first in an effort to eventually wind up with a deformed objective function surface with only global minima. The stochastic tunneling method of Wenzel and Hamacher[12] is a method that also deforms the objective function surface using a nonlinear transformation. The nonlinear transformation is

$$1 - \exp[-\gamma(f(x) - f_0)]$$

where γ is a tunneling parameter, $f(x)$ is the function whose global minimum is sought, and f_0 is the current lowest value of the objective function. Finally, we mention the basin hopping method of Wales and Doye,[13] where the objective function surface is deformed or transformed using local conjugate gradient minimizations (or quenches) after each Monte Carlo step on the objective function landscape. This type of deformation results in an up-and-down staircase structure to the objective function surface.

2. A Motivating Example

This section introduces a sample problem of a reactive catalyst pellet known to exhibit strong nonlinearity and solution multiplicity. The method of Orthogonal Collocation over Finite Elements (OCFE) for the numerical solution of the partial differential equations (PDEs) representing heat and mass transport in the spherical catalyst pellet is described. The use of the terrain methodology as described by Lucia and coworkers[6,7] to find all unconstrained and constrained minima and saddle points of the least-squares function is also explained. All calculations were performed in double-precision arithmetic, using both a Dell High Precision 670 workstation with a Lahey−Fujitsu (LF95) compiler and a Gateway personal computer with a Pentium III processor and Lahey LF77/90-EM32 compiler. Also, a trust region radius of 0.1 and a convergence tolerance of $||g|| = ||\mathbf{J}^T F|| \leq 10^{-6}$ (where $\mathbf{J}$ is the Jacobian matrix of F) were used in all cases.

2.1. Reaction and Diffusion in Catalyst Pellets. Many industrial reactors involve heterogeneous reaction kinetics of packed catalytic pellets in fixed-bed reactors, as illustrated in eq 1. A single catalyst pellet of radius R can be treated as a porous medium through which reactants diffuse while reactions occur simultaneously.

$$\mathrm{A} \xrightarrow[\Delta H]{\text{catalyst}} \mathrm{B} \tag{1}$$

The species and energy balances for diffusive transport inside the pellet can be written as given in eqs 2−6, which are given in the work by Villadsen and Michelsen.[14]

$$\text{species balance:} \quad D_{\epsilon z} \nabla^2 C_\mathrm{A} + r_\mathrm{A} = 0 \tag{2}$$

$$\text{heat balance:} \quad K_{\epsilon z} \nabla^2 T + r_\mathrm{A} \Delta H = 0 \tag{3}$$

Arrhenius reaction rate:

$$r_\mathrm{A} = -k_\mathrm{ref} \exp\left[\frac{-E}{R_\mathrm{g} T_\mathrm{ref}}\left(\frac{T_\mathrm{ref}}{T_\mathrm{s}} - 1\right)\right] C_\mathrm{A,s} \tag{4}$$

$$\text{known surface concentration:} \quad C_\mathrm{A}|_{r=R} = C_\mathrm{A,s} \tag{5a}$$

$$\text{known surface temperature:} \quad T|_{r=R} = T_\mathrm{s} \tag{5b}$$

$$\text{symmetrical boundary conditions:} \quad \nabla C_\mathrm{A}|_{r=0} = \nabla T|_{r=0} = 0 \tag{6}$$

At the surface, concentration and temperature can be given by a Dirichlet boundary condition such as that in eq 5. Because of symmetry, the mass and energy flux at the center of the catalyst pellet is zero, as shown in eq 6. The system described by eqs 2−6 represents the nonlinear PDE system for coupled heat and mass transfer in a spherical non-isothermal catalyst pellet. After inserting the temperature profile into the species balance, eqs 2−6 can be written in terms of the dimensionless concentration y ($y = C_\mathrm{A}/C_\mathrm{A,s}$), the dimensionless pellet radius x ($x = r/R$), and dimensionless constants γ, β, and ϕ. (See Appendix A (or Weisz and Hicks[15]) for a detailed derivation.)

dimensionless non-isothermal species & heat transport:

$$\frac{d^2y}{dx^2} + \frac{2}{x}\frac{dy}{dx} - \phi^2 y \exp\left[\frac{\gamma\beta(1-y)}{1+\beta(1-y)}\right] = 0 \tag{7}$$

$$\text{known surface concentration and temperature:} \quad y|_{x=1} = 1 \tag{8}$$

$$\text{symmetrical boundary condition:} \quad \left.\frac{dy}{dx}\right|_{x=0} = 0 \tag{9}$$

The overall reaction rate in a catalytic pellet is often expressed by the effectiveness factor (η), which measures the total reaction rate as a scalar multiple of a homogeneous first-order reaction at the surface concentration. The effectiveness factor for a spherical pellet is calculated via the integration of eq 7 and the Thiele modulus (from Weisz and Hicks[15]), as shown in eq 10.

$$\eta = \frac{3}{\phi^2}\left.\frac{dy}{dx}\right|_{x=1} \tag{10}$$

For coupled heat and mass transfer with reactions, the pellet concentration profiles and, thus, the effectiveness factor η exhibit multiplicity, even for linear reaction rate laws, as given in Figure 1. Multiplicity means that, for identical conditions given by the dimensionless parameters γ, β, and ϕ, the effectiveness factor η can assume several distinct, yet physically meaningful, solutions.[16] It is desirable to identify all distinct solutions, as

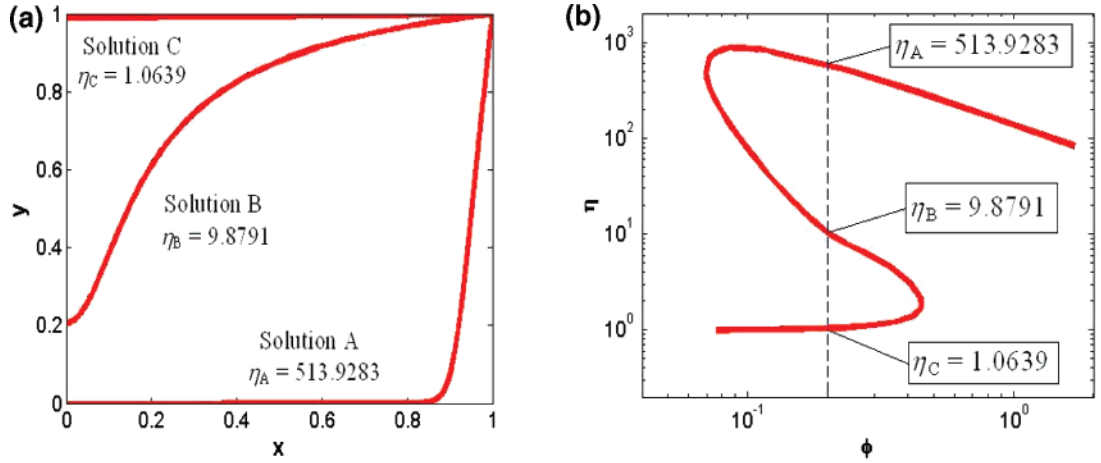

Figure 1. Depiction of multiple steady states for conditions $\gamma = 30$, $\beta = 0.6$, and $\phi = 0.2$: (a) the three concentration profiles (y) reproduced with the shooting method of Weisz and Hicks;[15] (b) the η-ϕ curve that displays three possible effectiveness factors, corresponding to these three concentration profiles and identical boundary conditions.

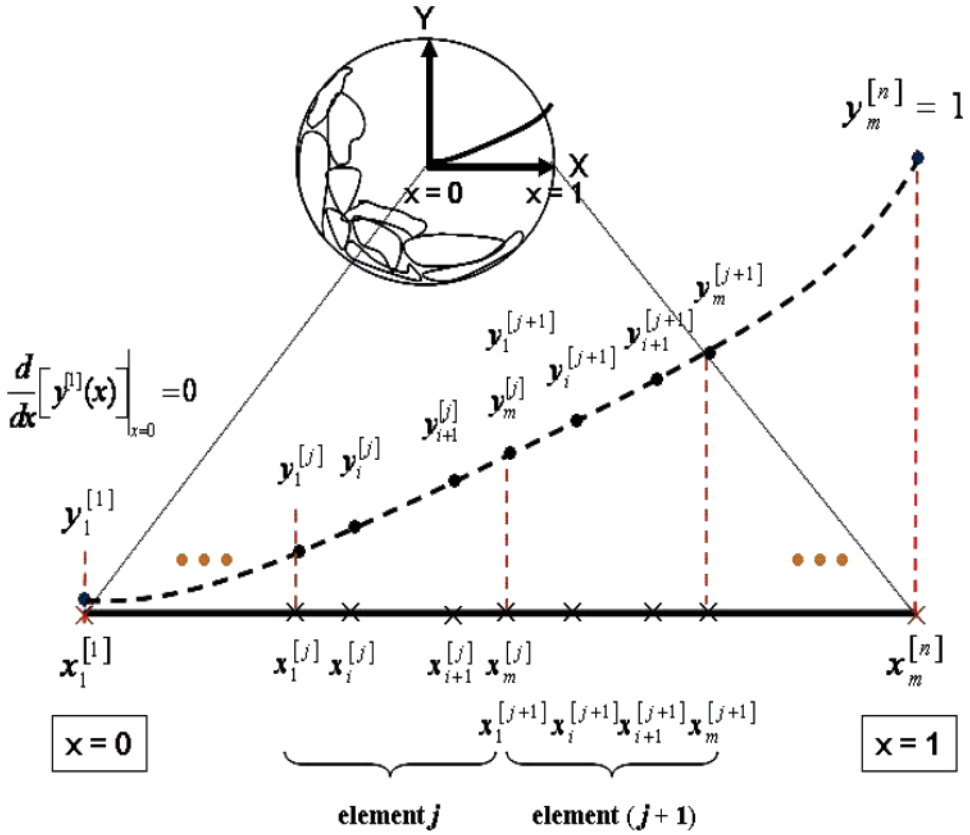

Figure 2. Division of the spherical catalyst pellet ($x = 0$ to $x = 1$) into n finite elements. Each element is further divided into m nodes, corresponding to the roots of the mth order Jacobi polynomial. The x-axis denotes the dimensionless radius (x) and the y-axis represents for the dimensionless concentration (y).

shown for the case of three solutions for $\gamma = 30$, $\beta = 0.6$, and $\phi = 0.2$ in Figure 1. Currently, both trial-and-error shooting methods[17,18] and a direct method that combines numerical integration and interval analysis[19] are available to find all solutions. Next, we will show a collocation method to be used with the new barrier-terrain method that will identify all solutions without resorting to shooting.

2.2. Discretization of the Pellet Equations. Concentration profile PDEs and effectiveness factor equations can be discretized with orthogonal collocation over finite elements (OCFE). The OCFE approximation to the boundary value problem given by eqs 7−9 divides the dimensionless radius domain $x \in [0,1]$ into n finite elements. Within each element, suitable orthogonal base functions—such as the Lagrangian polynomials $l_i^{[j]}(x)$ depicted in Figure 2—approximate the true profiles such that the integral approximation error over the element is minimized.[20,21] (For details on node selection, see the work of Villadsen and Michelsen.[14]) The approximate polynomial concentration profile in each element j can be written as a sum of base polynomials with unknown coefficients $y_i^{[j]}$, as shown in eq 11:

$$y^{[j]}(x) = \sum_{i=1}^{m} l_i^{[j]}(x)\, y_i^{[j]} \qquad (\text{for } j = 1, ..., n) \qquad (11)$$

where

$$l_i^{[j]}(x) = \prod_{\substack{k=1 \\ k\neq i}}^{m} \frac{x - x_k^{[j]}}{x_i^{[j]} - x_k^{[j]}}$$

Inserting the polynomial concentration profile for the *j*th element given by eq 11 into eq 7 gives eq 12.

$$\frac{d^2}{dx^2}[y^{[j]}(x)] + \frac{2}{x_i^{[j]}}\frac{d}{dx}[y^{[j]}(x)] - \phi^2 y^{[j]}(x) \exp\left[\frac{\gamma\beta(1 - y^{[j]}(x))}{1 + \beta(1 - y^{[j]}(x))}\right] = 0 \quad (\text{for } i = 2, ..., m-1; j = 1, ..., n) \quad (12)$$

After inserting the first and second derivatives of the base polynomials, eq 13 holds for the interior of each element.

$$\sum_{i=1}^{m} l_i^{[j]\prime\prime}(x_i^{[j]})\, y_i^{[j]} + \sum_{i=1}^{m} l_i^{[j]\prime}(x_i^{[j]}) y_i^{[j]} - \phi^2\, y^{[j]}(x) \exp\left[\frac{\gamma\beta(1 - y^{[j]}(x))}{1 + \beta(1 - y^{[j]}(x))}\right] = 0 \quad (\text{for } i = 2, ..., m-1; j = 1, ..., n) \quad (13)$$

At the intersection of two elements, eqs 14 and 15 enforce zero and first-order continuity between the concentration profiles, to ensure smooth transitions.

C^0, continuity of the profile from j to $j+1$:

$$y_i^{[j]}(x_m^{[j]}) = y_i^{[j+1]}(x_1^{[j+1]}) \quad (\text{for } j = 1, ..., n) \quad (14)$$

C^1, continuity of the profile from j to $j+1$:

$$\frac{d}{dx}[y^{[j]}(x)]_{x=x_m^{[j]}} = \frac{d}{dx}[y^{[j+1]}(x)]_{x=x1_i^{[j+1]}} \quad (15)$$

Finally, the boundary condition in eq 9 for the first node of the first element ($x = 0$) can now be written as shown in eq 16. Similarly, the last node of the last element of the boundary condition in eq 8 becomes eq 17 for the final node ($x = 1$).

$$\sum_{i=1}^{m} l_i^{[1]\prime}(x)|_{x=0} y_i^{[1]} = 0 \quad (16)$$

$$\sum_{i=1}^{m} l_i^{[n]}(x)|_{x=1} y_i^{[n]} = 1 \quad (17)$$

Thus, we finally have a system of $n(m-2) + 1 + 1 + (n-1) + (n-1) = nm$ equations in the nm unknown coefficients of the base polynomials. The objective of the terrain method is to identify *all sets of values* $y_i^{[j]}$ that solve the equation set described by eqs 13−17 simultaneously. As stated previously, in certain parameter ranges, more than one solution may solve the highly nonlinear equation set.

2.3. One-Point Collocation of a Spherical Catalyst Pellet. Application of collocation with two elements and three nodes gives the algebraic equations $f(y) = 0$ as represented in eqs 18−23, which contain four linear and two nonlinear equations. Here, the equation set described by eqs 13−17 is written over the elements [0, 0.5] and [0.5, 1] with the nodes at [0, 0.25, 0.5] and [0.5, 0.75, 1], as depicted in Figure 3.

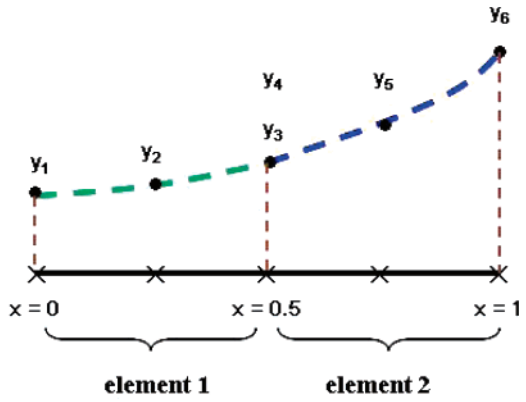

Figure 3. Division of the spherical catalyst pellet into two finite elements [0, 0.5] and [0.5, 1]. The element [0, 0.5] has collocation nodes at $x = 0$, $x = 0.25$, and $x = 0.5$ and the element [0.5, 1] has the collocation nodes at $x = 0.5$, $x = 0.75$, and $x = 1$.

$$f_1 = 6y_1 + 8y_2 - 2y_3 = 0 \quad (18)$$

$$f_2 = -32y_2 + 32y_3 - \phi^2 y_2 \exp\left[\frac{\gamma\beta(1 - y_2)}{1 + \beta(1 - y_2)}\right] = 0 \quad (19)$$

$$f_3 = 10.666667y_4 - 32y_5 + 21.333333y_6 - \phi^2 y_5 \exp\left[\frac{\gamma\beta(1 - y_5)}{1 + \beta(1 - y_5)}\right] = 0 \quad (20)$$

$$f_4 = y_4 - y_3 = 0 \quad (21)$$

$$f_5 = -6y_4 + 8y_5 - 2y_6 - 2y_1 + 8y_2 - 6y_3 = 0 \quad (22)$$

$$f_6 = y_6 - 1 = 0 \quad (23)$$

Elimination of y_1, y_4, and y_6 gives a system of two nonlinear equations in two unknown variables (i.e., the y variables, which denote the dimensionless concentration along the radial direction of the pellet). The reduced model equations are

$$F_1 = -32y_2 + 32y_3 - \phi^2 y_2 \exp\left[\frac{\gamma\beta(1 - y_2)}{1 + \beta(1 - y_2)}\right] = 0 \quad (24)$$

$$F_2 = 10.666667y_3 - 32y_5 + 21.333333 - \phi^2 y_5 \exp\left[\frac{\gamma\beta(1 - y_5)}{1 + \beta(1 - y_5)}\right] = 0 \quad (25)$$

where

$$y_3 = \frac{8y_5 - 2 + 8y_2}{12} - \left(\frac{8}{36}\right)\left(\frac{18}{17}\right)y_2 \quad (26)$$

Throughout this manuscript, we used parameter values of $\gamma = 30$, $\beta = 0.6$, and $\phi = 0.2$ and the bounds on the unknown variables were $0 \le y_2, y_5 \le 1$. Note that the conditions $0 \le y_1, y_3, y_4, y_6 \le 1$ should also be satisfied, although these variables have been eliminated from the optimization calculations.

2.4. Summary of the Terrain Method. Terrain methods have been described in detail elsewhere in the literature (e.g., Lucia and Yang[6,7]) and are briefly summarized here for the purpose of continuity. Terrain methods are used to locate sets of

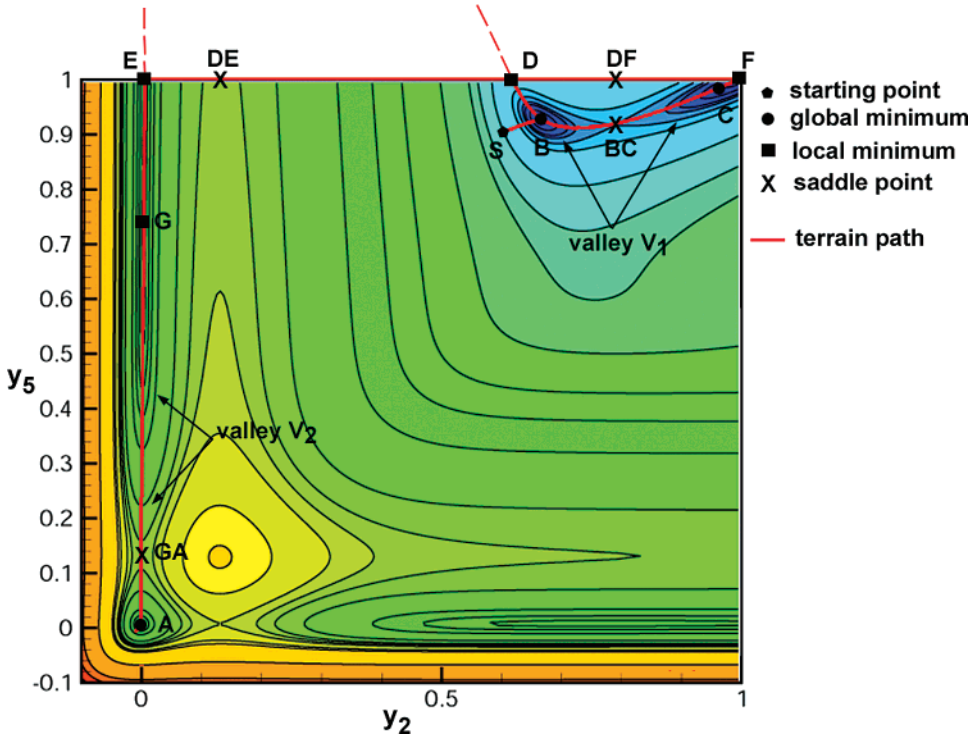

Figure 4. Level sets for a catalyst pellet problem (two elements, three nodes).

stationary and singular points of a general C^3 objective function (OBJ), subject to bounds on the optimization variables.

For the problems in this paper, the OBJ is the least-squares function given by

$$\text{OBJ} = F^{\mathrm{T}}F = \sum_{i=1}^{n} [F_i^{\,2}]^{1/2} \tag{27}$$

They do this by following valleys and moving up and down the landscapes of $g^{\mathrm{T}}g$ and OBJ, where g is the gradient of OBJ. The method used for downhill calculations, either initially or when moving downhill from a saddle point to a minimum, is a standard Newton-based trust region method with automatic step size adjustment so that Newton steps are taken at the end and quadratic convergence is achieved. Uphill calculations, on the other hand, follow the Newton vector field along the valley and use a fixed step size. The terrain method compensates for any drift from a valley (V) by intermittently solving a sequence of general nonlinearly, constrained optimization problems:

$$\text{V} = \min g^{\mathrm{T}}\mathbf{H}^{\mathrm{T}}\mathbf{H}g \tag{28}$$

$$\text{such that } g^{\mathrm{T}}g = L \quad \text{for all } L \in \Lambda$$

where $\mathbf{H}$ denotes the Hessian matrix of the OBJ, L is any given value (or level) of $g^{\mathrm{T}}g$, and Λ is some collection of contours. The nonlinear programming problem in eq 28 defines what are called uphill corrector steps. These corrector steps serve the purpose of forcing iterates back to the valley and are solved using a successive quadratic programming (SQP) method. At any stationary point, eigenvalues and eigenvectors are calculated to determine the character of that stationary point and whether the next direction to be explored should be uphill or downhill. In particular, uphill movement from any minimum is always initiated in the eigen-direction associated with the smallest positive eigenvalue, whereas the eigen-direction associated with the largest negative eigenvalue is used to move downhill from any saddle point. Our terrain methodology also keeps track of where it has been on the objective function landscape and, in this way, one can avoid recalculating previously determined stationary points. Convergence to singular points, either uphill or downhill, is accomplished using a second-order Newton method. Finally, termination occurs when the algorithm encounters a pair of bounds on one or more of the optimization variables. Thus, in summary, terrain methods require (i) reliable downhill equation solving; (ii) reliable and efficient computation of singular points; (iii) efficient uphill movement, comprised of predictor−corrector calculations; (iv) reliable and efficient eigenvalue-eigenvector computations; (v) effective bookkeeping; and (vi) a termination criterion to decide when the computations have been completed.

The stationary points for this example were determined using the terrain method, and the numerical values of the unknown variables and the least-squares function, along with the number of function, gradient, and Hessian matrix calls and computer time, are shown in Table 1. Note that there are three unconstrained global minima (i.e., points where $F^{\mathrm{T}}F = 0$ and $F = 0$), three unconstrained saddle points (i.e., $g = \mathbf{J}^{\mathrm{T}}F = 0$ but $F \neq 0$, which means $\mathbf{J}$ is singular), one unconstrained local minimum ($\mathbf{J}$ is also a singular point), three constrained minima along the $y_5 = 1$ axis, and two constrained saddle points along the $y_5 = 1$ axis. Also note that the terrain method requires 1106 function, gradient, and Hessian matrix evaluations to find all unconstrained and constrained stationary points of physical interest. The time needed for these calculations was 0.21 s, using the Pentium III computer. Figure 4 shows the terrain path for the results in Table 1.

2.5. Problem Attributes. Ignoring, for the moment, the constraint difficulties described in the previous section and treating solution A as a solution, it is of some interest to highlight the problem characteristics for this example, because, as the reader will learn, these attributes are actually generic, in the sense that they carry over to collocation models of the same spherical catalyst pellet problem with larger numbers of nodes

Table 1. Two-Dimensional (2-D) Optimization Results for a Two-Element, Three-Node Spherical Catalyst Pellet Model

stationary point	y_2	y_5	F^TF	calls[a]	time[b] (s)
global minimum B	0.66594	0.92606	3.369×10^{-8}		
saddle point BC	0.78928	0.91759	1.28150		
global minimum C	0.99313	0.99685	2.191×10^{-7}	342	0.05
constrained minimum D	0.62142	1.00000	3.76480		
saddle point DE	0.13050	1.00000	1.911×10^{4}		
constrained minimum E	0.00570	1.00000	25.3108		
saddle point DF	0.75043	1.00000	9.14802		
constrained minimum F	0.99753	1.00000	2.741×10^{-3}	347	0.05
local minimum G	0.00354	0.72383	0.091834		
saddle point GA	−0.00079	0.13126	1.868×10^{4}		
global minimum A	−0.00175	0.00656	6.685×10^{-13}	417	0.11

[a] Calls means evaluations of the function (F), gradient ($g = \mathbf{J}^TF$), and Hessian matrix ($\mathbf{H}$), where the Hessian matrix is given by $\mathbf{H} = \mathbf{J}^T\mathbf{J} + \Sigma F_i\nabla^2F_i$. [b] Time given in seconds on a Pentium III computer.

and elements. To do this, we draw the reader's attention to Figure 4, which give the level sets or contours for this reduced space catalyst pellet example in two dimensions and illustrates the following problem characteristics.

(1) There is a smooth and simple curved valley, V_1, that connects two of the three solutions within the feasible region.

(2) There is a "second" straight valley, V_2, which runs along the y_5-axis that contains a solution that is something of an outlier.

(3) Evidence of these valleys (V_1 and V_2) can be found along the edges of the feasible region defined by the constraints $y_5 = 1$ and $y_2 = 1$.

(4) Valleys V_1 and V_2 are separated by a local maximum and an associated ridge that runs parallel to V_2.

5) The valleys, V_1 and V_2, are actually *not* connected unless an edge of the feasible region is considered part of the terrain path, and then the path is not smooth.

Problem characteristics 1−4 are illustrated in Figure 4. The terrain calculations depicted in Figure 4 begin at the starting point S, finding three unconstrained stationary points in valley V_1—a global minimum (point B), a saddle point (BC), and a second global minimum (C)—before striking the boundary at points D and F respectively. The terrain method then searches along the constraint $y_5 = 1$ for evidence of a "second" valley and finds that evidence by computing the constrained saddle point DE and, subsequently, the constrained minima at points E and F. Because points C and F are very close, point E is chosen as the marker for this "second" valley. The calculations then determine the eigenvalues of the Hessian matrix,

$$\mathbf{H} = \mathbf{J}^T\mathbf{J} + \sum F_i\nabla^2F_i$$

at point E in two dimensions. Because the smallest eigenvalue of $\mathbf{H}$ is $\lambda = 617.650$ and has an associated eigenvector (6.28136×10^{-5}, 0.999937) that is orthogonal to the constraint $y_5 = 1$, this indicates that movement should be into the feasible region—so the constraint $y_5 = 1$ is relaxed. From here, the terrain method in the y_2−y_5 variable space easily finds the local minimum at point G, saddle point GA, and the global minimum at point A along valley V_2.

Characteristic 5 presents the most significant difficulty. Figure 4 clearly indicates that the valleys V_1 and V_2 are not connected within the feasible region. Even if the feasible region is enlarged, these valleys are also not connected. This can be illustrated by inspecting the behavior of

$$f = \exp\left[\frac{\gamma\beta(1 - y_5)}{1 + \beta(1 - y_5)}\right] \qquad \text{for } y_5 > 1$$

(i.e., along the valley V_1 as it exists the feasible region). This function is well-defined for the range $0 < y_5 < 2.667$, because as $y_5 \rightarrow 2.667$, $f \rightarrow 0$. At $y_5 = 2.667$, f is undefined, at least in finite-length arithmetic. For $y_5 > 2.667$, it is easily seen that $f = \exp[\gamma\beta(1 - y_5)/(1 + \beta(1 - y_5))]$ takes on extremely large positive values (effectively ∞) and remains large for very large values of y_5 (e.g., for $y_5 = 50{,}000$, the quantity $\exp[\gamma\beta(1 - y_5)/(1 + \beta(1 - y_5))]$ is still 10^{13}). Thus, valleys V_1 and V_2 are not smoothly connected. The connection that contains an edge of the feasible region shown in Figure 4 is artificial, not smooth, and ad hoc at best! Thus, there is *no* smooth connection between solution A and solutions B and C, and this presents a fundamental problem for a method such as the terrain method, which is built on following smoothly connected valleys. There are also difficulties associated with the computation of the derivatives of functions such as f that involve exponential quantities such as $\exp\{\gamma\beta(1 - y_5)/(1 + \beta(1 - y_5))]/[1 + \beta(1 - y_5)]\}$, which go to 0 times ∞ or 0/0 as y_5 approaches 2.667 and cannot be removed by application of L'Hospital's rule.

Remark. Starting the optimization calculations from the initial guess $y = (y_2, y_5) = (0, 0)$ easily traces the terrain path in the reverse direction (i.e., starting from solution A and ending with solution C) and thus calculates the unconstrained and constrained stationary points shown in Table 1 from bottom to top.

2.6. Variable Elimination and Embedded Constraint Difficulties. It is important to note that constraint violations occur during the process of finding solution A for the model given by eqs 24−26. Specifically, the variables y_3 and y_4 take on significantly negative values that violate their respective lower bounds during the solution process. In fact, if one uses eq 26, it is easily seen that $y_3 = y_4 = -0.172661$ at solution A, which clearly violate the bounds $y_3, y_4 \geq 0$. Moreover, the lower bound on y_1 is also violated along the constraint $y_5 = 1$ on the interval $0 \leq y_2 \leq 0.1498$ and in traversing valley V_2. We believe that these constraint violations are, in part, due to the coarse grid used in the collocation modeling. Thus, while solution A is not a solution in the full space of the y variables, we treat it as such in the ensuing discussions, because it is a solution when larger collocation models are used. On the other hand, no constraint violations occur along valley V_1.

3. Creating Smooth Terrain Paths Using Logarithmic Barrier Functions

The ad hoc approach of searching edges of the feasible region described in the previous section is unsatisfactory for several reasons, not the least of which is that it does not find all solutions when larger collocation models are used. Moreover, when the number of nodes and elements increases, there are many edges to the feasible region and it becomes much more challenging to find the correct edge or edges to search as part of any terrain

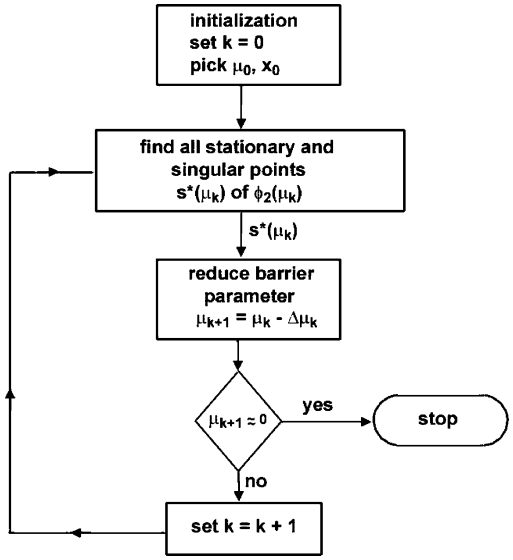

Figure 5. Flowchart for the barrier-terrain algorithm.

path. What we would prefer is a method that automatically creates appropriate and smoothly connected valleys so that all physically meaningful solutions can be found. One way to do this is to use logarithmic barrier functions.

Here, we show how to use logarithmic barrier functions in a unique way: to construct smooth valleys between solutions that otherwise do not exist. The central idea in this work is very simple. To create a terrain path, we use the following augmented objective function:

$$\phi_2 = \mathrm{OBJ} - \mu[\sum_{i=1}^{n} \ln(y_i^{\mathrm{U}} - y_i) + \ln(y_i - y_i^{\mathrm{L}})] \qquad (29)$$

where OBJ is the original given objective function (e.g., eq 28), ϕ_2 is an augmented objective function, y^{U} and y^{L} are vectors of upper and lower bounds on all optimization variables, and $\mu \geq 0$ is a barrier parameter such that $\lim \mu \rightarrow 0$. Note that a large initial value of μ gives a unique minimum for ϕ_2 whereas for $\mu = 0$, the stationary points of ϕ_2 are those of OBJ. Also, an iterative updating technique for driving the barrier parameter toward zero is needed, and we represent this updating strategy by

$$\mu_{k+1} = \mu_k - \Delta\mu_k \qquad (30)$$

Remark. For the catalyst pellet problem and some set of *appropriately* chosen intermediate values of the barrier parameter bounded away from zero, there will exist a smooth valley that connects a variety of stationary points on ϕ_2 that, qualitatively, "look like" solutions on OBJ $= F^{\mathrm{T}}F$. This fact is true using simple continuous differentiability arguments. Once a smooth terrain path on ϕ_2 has been found, then all stationary points are tracked using the terrain method as the value of μ approaches 0. This will be illustrated shortly.

3.1. A Simple Barrier-Terrain Algorithm. Because there is generally no rigorous way to decide how large the barrier parameter must be and because stationary points can appear and disappear as μ changes, we must be conservative in finding all solutions—and this has led to a simple barrier-terrain algorithm.

A Barrier-Terrain Algorithm:

(1) Given the C^3 objective function, OBJ, with simple bounds on variables, construct the augmented objective function ϕ_2, as given by eq 29.

(2) Set $k = 0$ and pick $\mu_0 \gg 0$, choose a starting point y_0, and use the terrain method to find as many stationary points of $\phi_2(\mu_0)$ as desired. Let the initial set of stationary points be defined as "$s^*(\mu_0)$".

(3) Using the stationary points, $s^*(\mu_k)$, gradually reduce the barrier parameter by setting $\mu_{k+1} = \mu_k - \Delta\mu_k$ and use the terrain method to find the stationary points of $\phi_2(\mu_{k+1})$. Call this set of stationary points "$s^*(\mu_{k+1})$".

(4) Set $k = k + 1$ and repeat step 3 until $\mu \approx 0$.

Step 1 simply constructs the augmented objective function, ϕ_2. Step 2, on the other hand, finds an initial set of stationary points to the augmented objective function using the terrain

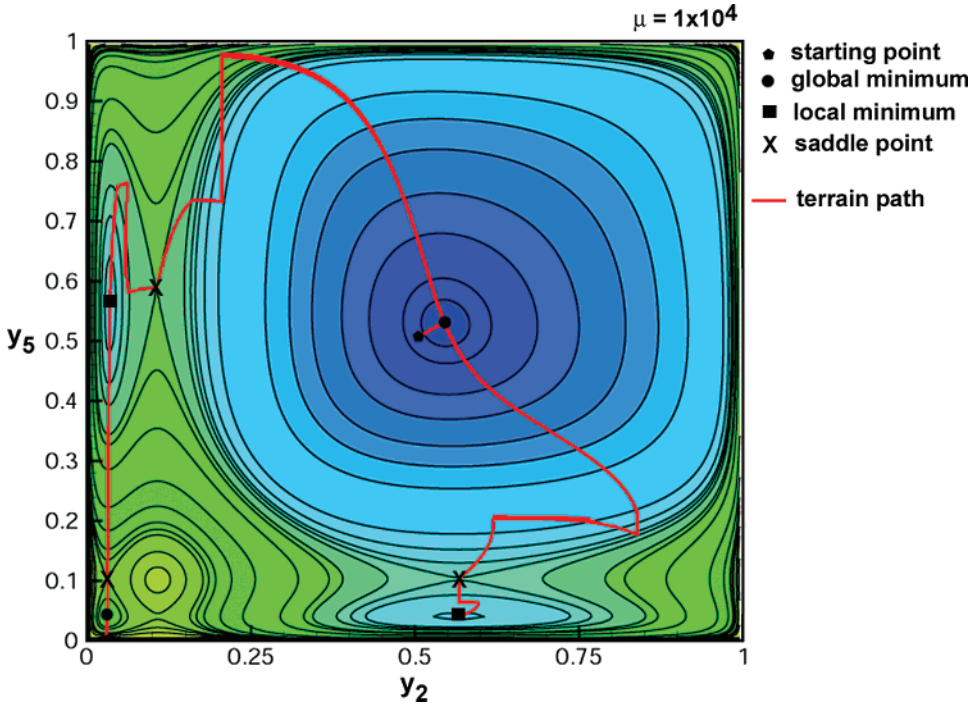

Figure 6. Barrier-terrain contours for catalyst pellet problem (two elements, three nodes; $\mu = 10^4$).

Table 2. Barrier Iteration #1 Results for a Two-Element, Three-Node Spherical Catalyst Pellet Model

stationary point	y_2	y_5	ϕ_2[a]	calls	time (s)
global minimum B	0.545228	0.528511	2.81550×10^4	10	
saddle point	0.567631	0.103146	5.51661×10^4	1325	
minimum	0.565359	0.040443	5.523443×10^4	581	
saddle point	0.105983	0.584917	5.85350×10^4	656	
local minimum G	0.034509	0.556522	5.39222×10^4	865	
saddle point GA	0.031247	0.102852	8.27533×10^4	1158	
local minimum A	0.030762	0.039644	7.97794×10^4	1781	2.31

[a] $\mu = 10^4$.

Table 3. Barrier Iteration #2 Results for a Two-Element, Three-Node Spherical Catalyst Pellet Model

stationary point	y_2	y_5	ϕ_2[a]	calls	time (s)
global minimum B	0.689207	0.655429	3.39929×10^2	22	
saddle point	0.893870	0.130703	1.82511×10^4	1047	
local minimum	0.732126	0.008698	1.03211×10^3	1401	
saddle point GA	0.130287	0.008070	2.65056×10^4	1776	
local minimum A	0.001595	0.007454	1.24825×10^3	2332	2.14

[a] $\mu = 100$.

Table 4. Barrier Iteration #3 Results for a Two-Element, Three-Node Spherical Catalyst Pellet Model

stationary point	y_2	y_5	ϕ_2[a]	calls	time (s)
global minimum B	0.680596	0.738428	2.78162×10^2	29	
saddle point	0.130298	0.986979	1.97185×10^4	584	
local minimum G	0.004396	0.695471	5.68583×10^2	842	
saddle point GA	0.001717	0.130939	1.94227×10^4	1287	
local minimum A	0.001364	0.007294	1.01956×10^3	1832	2.25

[a] $\mu = 80$.

method. Here, in our opinion, it is important to pick a value of μ that is sufficiently large so that the augmented objective function is convex on the feasible region and ϕ_2 has a unique minimum. In step 3, the barrier parameter is reduced and the previous set of stationary points ($s^*(\mu_k)$) is used to track the solutions on $\phi_2(\mu_{k+1})$. The algorithm terminates when the barrier parameter is sufficiently close to zero. Figure 5 gives a flowchart for the barrier-terrain algorithm.

3.2. A Complete Illustration. In this section, we continue with the two-dimensional example of the two-element, three-node collocation model for the spherical catalyst pellet problem (i.e., eqs 24−26 with constraints $0 \leq y_2, y_5 \leq 1$) and take the reader through a *complete* set of barrier-terrain optimization calculations. All calculations were performed in double-precision arithmetic on a Pentium III system using the Lahey LF77/90-EM32 compiler. The convergence tolerance for the gradient of ϕ_2 was $\epsilon = 10^{-6}$, and the initial step size for the terrain method was $h = 0.05$. Analytical first and second derivatives of ϕ and the barrier term in eq 29 were used.

3.2.1. Barrier Iteration #0. We begin by selecting $\mu_0 = 10^5$. Using the starting point $y = (0.01, 0.01)$, we calculate the unique minimum of the $y^* = s^*(\mu_0) = (0.508214, 0.504800)$ on the surface $\phi_2(\mu_0)$ in 1264 function evaluations and 0.87 s of computer time. Here, ϕ_2^* has a value of 2.77865×10^5. We note that only 18 iterations were actually required to find $s^*(\mu_0)$, and the remainder of the computational work was spent following the valley in the feasible region, only to determine if there is a unique solution for this barrier parameter value.

Table 5. Barrier Iteration #4 Results for a Two-Element, Three-Node Spherical Catalyst Pellet Model

stationary point	y_2	y_5	ϕ_2[a]	calls	time (s)
global minimum B	0.680952	0.815708	1.46536×10^2	11	
saddle point	0.130392	0.993430	1.94453×10^4	638	
local minimum G	0.004002	0.707231	2.87010×10^2	910	
saddle point GA	0.001115	0.131067	1.90735×10^4	1378	
local minimum A	0.000817	0.006955	5.48634×10^2	1914	2.15

[a] $\mu = 40$.

Table 6. Barrier Iteration #5 Results for a Two-Element, Three-Node Spherical Catalyst Pellet Model

stationary point	y_2	y_5	ϕ_2[a]	calls	time (s)
global minimum B	0.681137	0.881188	3.93588×10^1	11	
saddle point	0.130463	0.998346	1.92130×10^4	722	
local minimum G	0.003669	0.718973	7.24160×10^1	979	
saddle point GA	0.000429	0.131174	1.87936×10^4	1487	
local minimum A	0.000258	0.006682	1.72472×10^2	1995	2.14

[a] $\mu = 10$.

3.2.2. Barrier Problem #1. We set $\mu_1 = 10^4$ and use $s^*(\mu_0) = (0.508214, 0.504800)$ as the starting point for the next set of terrain optimizations. Here, the terrain method finds five stationary points ($s^*(\mu_1)$) and five singular points on $\phi_2(\mu_1)$ in 1781 function and gradient calls and 2.31 s. (See Figure 6.) We note that the vertical parts of the terrain path that look out of place are actually smooth, computed paths along narrow singular valleys on g^Tg and are *not* indiscriminate "jumps" from one point to another on the surface of ϕ_2. The stationary points (i.e., minima and saddle points) and the corresponding values of ϕ_2 are shown in Table 2.

The cumulative function and gradient evaluations shown in Table 2 reflect the computational work to find singular points, which cannot be avoided, and in reaching the boundary of the feasible region. However, the *most* important aspect of barrier iteration #1 is the appearance of several stationary points and a smooth terrain path connecting them, as shown in Figure 6.

In fact, we note that global minimum B and local minimum A in Table 2 look like solution B and solution A, respectively, in Table 1.

3.2.3. Barrier Iteration #2. We continue by reducing μ to $\mu_2 = 100$ and use $s^*(\mu_1)$ to track stationary points on $\phi_2(\mu_2)$. In practice, it is sufficient to usually use only a few stationary points from $s^*(\mu_k)$ to find all stationary points in $s^*(\mu_{k+1})$, after the solution structure of the augmented objective function reveals itself. Here, we select *only* global min B in Table 2 to initialize terrain calculations for this barrier iteration. The minima and saddles of ϕ_2 are shown in Table 3.

The optimization results give a set of five stationary points and four singular points on $\phi_2(\mu_2)$ and require 2332 function and gradient calls and 2.14 s. Note that there is *still* a smooth connection from the regions that contain solution A and solution B, which is similar to that shown in Figure 6.

3.2.4. Barrier Iteration #3. Here, $\mu_3 = 80$ and we use the set $s^*(\mu_2)$ to track stationary points on $\phi_2(\mu_3)$. Again, we select the global min B in Table 3 to initialize the terrain calculations for this barrier iteration. A set of five stationary points and five singular points on $\phi_2(\mu_3)$ were found in 1832 function and gradient evaluations and 2.25 s. The stationary points are shown in Table 4, along with corresponding values of ϕ_2. Figure 7 shows the terrain path for these calculations.

Note there is still a smooth connection from the region that contains solution A and that which contains global min B, as

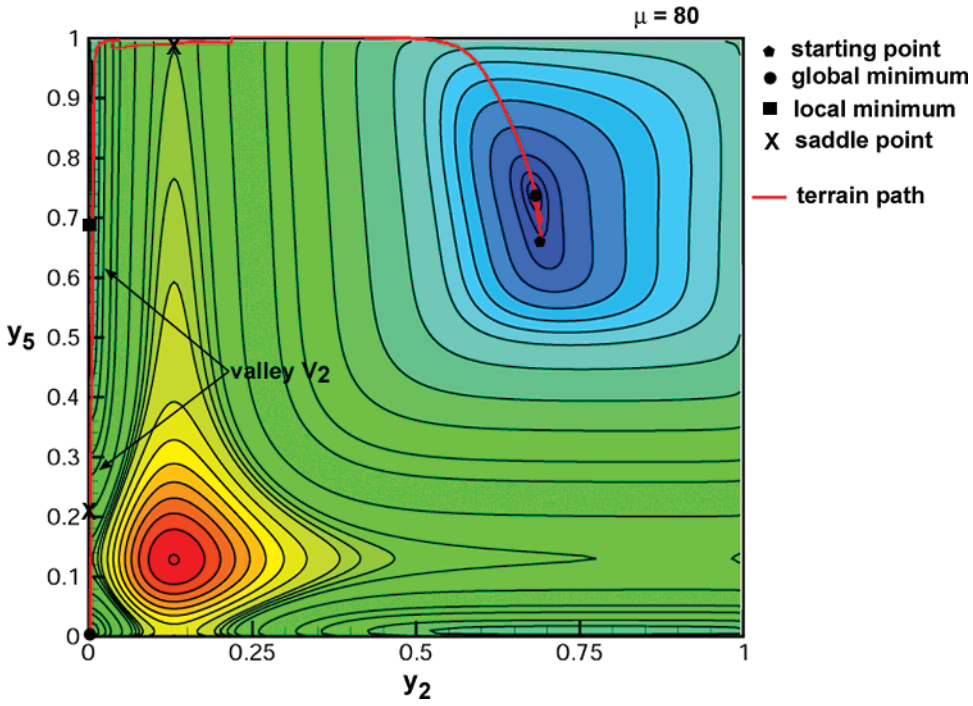

Figure 7. Barrier-terrain contours for catalyst pellet problem (two elements, three nodes; $\mu = 80$).

Table 7. Barrier Iteration #6 Results for a Two-Element, Three-Node Spherical Catalyst Pellet Model

stationary point	y_2	y_5	ϕ_2[a]	calls	time (s)
global minimum B	0.669784	0.918668	4.14129	12	
saddle point	0.130484	0.999834	1.91291×10^4	2850	
local minimum G	0.003561	0.723310	7.34424	6320	
saddle point GA	6.107×10^{-5}	0.131215	1.86989×10^4	8916	
local minimum A	2.895×10^{-5}	0.006596	46.7041	10,233	7.63

[a] $\mu = 1$.

shown in Figure 7. Also note that the contours of ϕ_2—in particular, valley V_2—and the terrain path are quite similar to that shown in Figure 4. The terrain path follows the boundary very close to a value of $y_5 = 1$. In addition, if one compares Figures 6 and 7, it is apparent that there is a distortion of the basin that surrounds the global minimum B that is occurring as μ gets smaller.

3.2.5. Barrier Iteration #4. We set $\mu_4 = 40$ and use the global min B in $s^*(\mu_3)$ to track stationary points on $\phi_2(\mu_4)$. Again, five stationary points and five singular points were located by the terrain method. The computational work that was required to find these stationary and singular points was 1914 function and gradient calls and 2.15 s. Table 5 provides some of the details for these optimization calculations.

3.2.6. Barrier Iteration #5. Here, $\mu_5 = 10$ and $s^*(\mu_4)$ is used to track stationary points on $\phi_2(\mu_5)$. Again, we select the global min B in Table 5 to initialize terrain calculations for this barrier iteration.

A set of five stationary points on $\phi_2(\mu_5)$ are shown in Table 6 and required 1995 function and gradient evaluations and 2.14 s. Note that a smooth connection from the region that contains solution A to that which contains global min B still exists.

3.2.7. Barrier Iteration #6. Here, $\mu_6 = 1$ and $s^*(\mu_5)$ is used to track stationary points on $\phi_2(\mu_6)$. Again, we select the global min B in Table 6 to initialize terrain calculations for this barrier iteration. The five stationary points on $\phi_2(\mu_6)$ required 10 233 function and gradient evaluations and 7.63 s to compute. The stationary points are shown in Table 7.

Table 8. Barrier Iteration #7 Results for a Two-Element, Three-Node Spherical Catalyst Pellet Model

stationary point	y_2	y_5	ϕ_2[a]	calls	time (s)
global minimum B	0.666391	0.925239	0.41796	10	
saddle point BC	0.792142	0.917706	1.71965	2882	
local minimum C	0.958472	0.979117	0.79499	6073	0.38
local minimum A	2.936×10^{-6}	0.006587	32.1099	814	2.08

[a] $\mu = 0.1$.

For these calculations, the integration step size was reduced to 0.01, because the barrier function begins to produce very tightly packed level curves along the boundaries of the feasible region. Note that there is still a smooth connection from the region that contains solution A to that containing global min B, which runs very close to the $y_5 = 1$ and then $y_2 = 0$ edges of the feasible region, and note that it is difficult to follow, as indicated by the number of function and gradient evaluations. Note also that the value of ϕ_2 for global min B, local min G, and local min A are approaching zero.

3.2.8. Barrier Iteration #7. Here, $\mu_7 = 0.1$ and $s^*(\mu_6)$ is used to track stationary points on $\phi_2(\mu_7)$. Again, we select the global min B in Table 7 to initialize terrain calculations for this barrier iteration. Here, three stationary points and two singular points were found on $\phi_2(\mu_7)$ in 6073 function and gradient calls and 0.38 s. The results of these optimizations are shown in Table 8 and Figure 8.

For these calculations, the integration step size was 0.01. Note that the terrain method found solutions very similar to solution

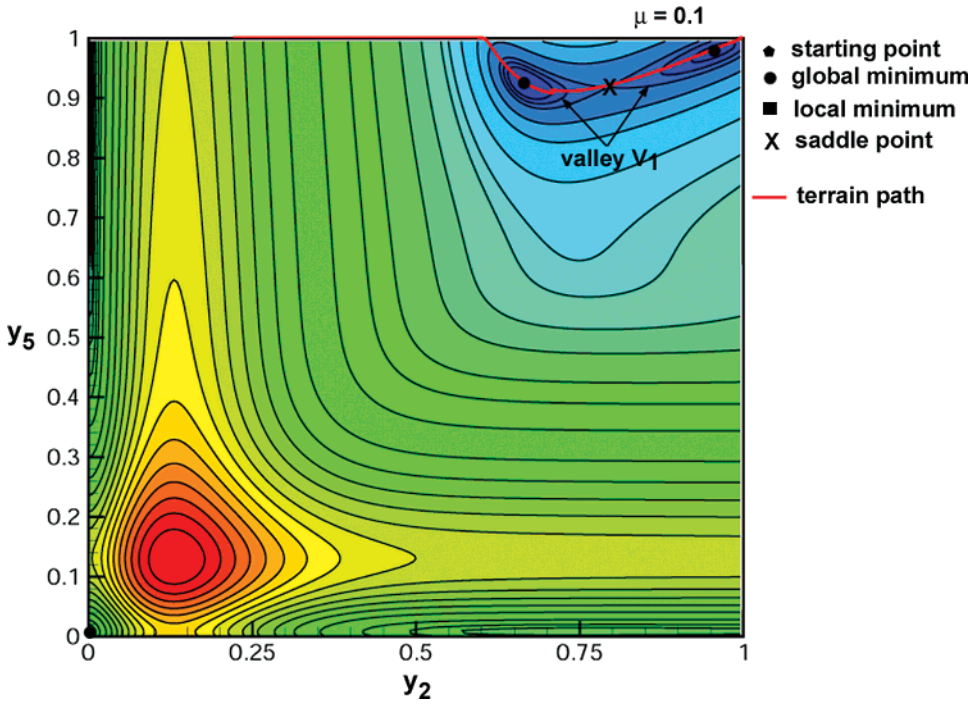

Figure 8. Barrier-terrain contours for catalyst pellet problem (two elements, three nodes; $\mu = 0.1$).

Table 9. Barrier Iteration #7 Results for a Two-Element, Three-Node Spherical Catalyst Pellet Model

stationary point	y_2	y_5	ϕ_2[a]	calls	time (s)
global minimum B	0.665992	0.925979	0.04183	11	
saddle point BC	0.789561	0.917603	1.32527	1088	
local minimum C	0.984255	0.992257	0.09614	10,235	0.65

[a] $\mu = 0.01$.

Table 10. Newton's Method Results for a Two-Element, Three-Node Spherical Catalyst Pellet Model

stationary point	y_2	y_5	F^TF	calls	time (s)
global minimum B	0.665947	0.926063	5.735×10^{-19}	7	0.00
local minimum C	0.993190	0.996880	1.270×10^{-22}	8	0.00

B, saddle point BC, and solution C in Table 1. We also note that, although there is a smooth connection between global minimum B and solution A, it cannot be calculated, because of the very tightly packed level curves along the boundary. On the other hand, only solution A can be calculated from local min A in Table 8; no other stationary or singular points were found and the computational work was 814 function and gradient calls. Finally, note that local min A in Table 8 still has a value of ϕ_2 that is quite far from zero, compared to those for global min B and local min C. This, coupled with the fact that local min A is very near to the edge of the feasible region and is evolving toward the boundary as μ approaches zero suggests that solution A will not turn out to be a solution to the original system of algebraic equations!

3.2.9. Barrier Iteration #8. Here, $\mu_8 = 0.01$ and $s^*(\mu_7)$ is used to track stationary points on $\phi_2(\mu_8)$. Here, we select the global min B *and* local min A in Table 8 to initialize the terrain calculations for this barrier iteration. From global min B, three stationary points and one singular point were found on $\phi_2(\mu_8)$ in 10 235 function and gradient calls and 0.65 s. No stationary points were found from local min A, and this is a correct result, because solution A has moved outside the feasible region for this value of the barrier parameter. See the discussions surrounding the results reported in Table 1 and illustrated in Figure 4. The results of these optimizations are shown in Table 9. For these calculations, the integration step size was reduced again to 0.005.

3.3. Finalizing the Barrier-Terrain Optimizations. The tightly packed contours around the boundary of the feasible region that occur with the use of logarithmic barrier functions as μ approaches zero challenge optimization methods. This is particularly a problem if there are solutions that lie very near to or on the boundary, such as solution C in Table 9. However, it is rather easy to monitor the evolution of $\phi = F^TF$, as a function of the barrier parameter μ, and, although it is a subjective decision, decide when to stop or simply use the last barrier solutions and switch to something like Newton's method to perform the final calculations for finding solutions to $F = 0$. For example, using the global min B and local min C in Table 9, it is easy to find the two solutions to $F = 0$ using Newton's method. These results are shown in Table 10 for an initial step size of $h = 0.05$.

3.4. Some Overall Comments. It is important to summarize the results thus far before moving to a larger example problem.

(1) A logarithmic barrier function was used to create smooth paths that connect all solutions or stationary points for some values of the barrier parameter when none exist on the given objective function surface. This smooth connection between valleys V_1 and V_2 exist from $\mu = 10^5$ to $\mu \approx 1$.

(2) A barrier-terrain method provides the ability to determine the number of solutions on the fly without the need for a priori knowledge of the solution structure. That is, when the barrier parameter is chosen to be large, then a unique solution can be found. Subsequently, as the barrier parameter is systematically reduced, stationary points on the augmented objective function appear (and possibly disappear) and low-lying valleys that connect these stationary points also evolve. Thus, the stationary

points can be reliably and efficiently followed by the terrain method.

(3) The barrier-terrain approach can require more computational effort than just the terrain method alone.

(4) One challenging disadvantage of the barrier-terrain approach is the very tight packing of level sets along the boundaries of the feasible region that occurs at small values of the barrier parameter. This has a tendency to make paths that do exist difficult to follow, because of severe ill-conditioning of the Jacobian and Hessian matrices.

4. Spherical Catalyst Pellet Model with Four Nodes and Five Elements

Here, a collocation model with five elements and four nodes results in a system of 10 linear algebraic equations and 10 nonlinear algebraic equations.

$$f_1 = -560.0006013y_1 - 450.159477y_2 + 1680.018038y_3 - 669.852549y_4 - \phi^2 y_2 \exp\left[\frac{\gamma\beta(1-y_2)}{1+\beta(1-y_2)}\right] = 0 \quad (31)$$

$$f_2 = -150.053159y_1 + 450.159477y_2 - 1680.018038y_3 + 1379.911720y_4 - \phi^2 y_3 \exp\left[\frac{\gamma\beta(1-y_3)}{1+\beta(1-y_3)}\right] = 0 \quad (32)$$

$$f_3 = 116.672077y_5 - 260.629618y_6 + 233.197543y_7 - 89.240002y_8 - \phi^2 y_6 \exp\left[\frac{\gamma\beta(1-y_6)}{1+\beta(1-y_6)}\right] = 0 \quad (33)$$

$$f_4 = -44.439109y_5 + 127.197493y_6 - 366.629667y_7 + 283.871283y_8 - \phi^2 y_7 \exp\left[\frac{\gamma\beta(1-y_7)}{1+\beta(1-y_7)}\right] = 0 \quad (34)$$

$$f_5 = 142.832077y_9 - 241.748521y_{10} + 158.251479y_{11} - 59.335035y_{12} - \phi^2 y_{10} \exp\left[\frac{\gamma\beta(1-y_{10})}{1+\beta(1-y_{10})}\right] = 0 \quad (35)$$

$$f_6 = -41.137162y_9 + 115.194849y_{10} - 284.805151y_{11} + 210.747464y_{12} - \phi^2 y_{11} \exp\left[\frac{\gamma\beta(1-y_{11})}{1+\beta(1-y_{11})}\right] = 0 \quad (36)$$

$$f_7 = 593.78736y_{13} - 907.995664y_{14} + 498.254336y_{15} - 184.04448y_{16} - \phi^2 y_{14} \exp\left[\frac{\gamma\beta(1-y_{14})}{1+\beta(1-y_{14})}\right] = 0 \quad (37)$$

$$f_8 = -160.498678y_{13} + 442.544542y_{14} - 963.705458y_{15} + 681.659593y_{16} - \phi^2 y_{15} \exp\left[\frac{\gamma\beta(1-y_{15})}{1+\beta(1-y_{15})}\right] = 0 \quad (38)$$

$$f_9 = 792.468507y_{17} - 1196.675063y_{18} + 640.059631y_{19} - 235.853076y_{20} - \phi^2 y_{18} \exp\left[\frac{\gamma\beta(1-y_{18})}{1+\beta(1-y_{18})}\right] = 0 \quad (39)$$

$$f_{10} = -213.320483y_{17} + 586.746946y_{18} - 1249.987748y_{19} + 876.561286y_{20} - \phi^2 y_{19} \exp\left[\frac{\gamma\beta(1-y_{19})}{1+\beta(1-y_{19})}\right] = 0 \quad (40)$$

$$f_{11} = -53.846154y_1 + 63.047326y_2 - 16.893480y_3 + 7.692308y_4 = 0 \quad (41)$$

$$f_{12} = y_5 - y_4 = 0 \quad (42)$$

$$f_{13} = y_9 - y_8 = 0 \quad (43)$$

$$f_{14} = y_{13} - y_{12} = 0 \quad (44)$$

$$f_{15} = y_{17} - y_{16} = 0 \quad (45)$$

$$f_{16} = -25.925926y_5 + 30.356120y_6 - 8.133898y_7 + 3.703704y_8 + 7.692308y_1 - 16.893480y_2 + 63.047326y_3 - 53.846154y_4 = 0 \quad (46)$$

$$f_{17} = -23.333333y_9 + 27.320508y_{10} - 7.320508y_{11} + 3.333333y_{12} + 3.703704y_5 - 8.133898y_6 + 30.356120y_7 - 25.925926y_8 = 0 \quad (47)$$

$$f_{18} = -43.750000y_{13} + 51.225953y_{14} - 13.725953y_{15} + 6.250000y_{16} + 3.333333y_9 - 7.320508y_{10} + 27.320508y_{11} - 23.333333y_{12} = 0 \quad (48)$$

$$f_{19} = -50.000000y_{17} + 58.543946y_{18} - 15.686803y_{19} + 7.142857y_{20} + 6.250000y_{13} - 13.725953y_{14} + 51.225953y_{15} - 43.750000y_{16} = 0 \quad (49)$$

$$f_{20} = y_{20} - 1 = 0 \quad (50)$$

4.1. Full Space Optimization Calculations. Using *only* the terrain methodology without a logarithmic barrier function, we have discovered that the five-element, four-node collocation model in the full space with 20 optimization variables is very similar in regard to solution structure to the two-element, three-node collocation model with two optimization variables that was discussed in previous sections, with some notable exceptions. The similarities include the following facts:

(1) There are three solutions or global minima. All three solutions are physically meaningful and can be verified independently using a shooting method.[15] However, not all solutions are connected by a single low-lying valley on the least-squares surface. These solutions lay in two disjointed valleys (V_1 and V_2).

(2) Valley V_1 is a simple curved valley that contains two global minima (B and C) and a saddle point (BC) between them.

(3) Valley V_2 contains a local minimum, a saddle point, and a global minimum—similar to points G, GA, and A in Figure 1.

On the other hand, the following conditions make the solution structure for this larger collocation model substantially different than the smaller reduced space collocation model:

(1) There really are *three* physically meaningful solutions within the feasible region.

(2) All solutions (A, B, and C) are constrained minima, not unconstrained global minima.

(3) The local minimum G and the saddle point GA lie well outside the feasible region.

Also, the computational effort required to find all solutions is demanding, because valleys V_1 and V_2 are extremely narrow and require frequent uphill, successive quadratic programming (SQP) corrector steps to follow. (See Lucia and Yang[6] for a detailed description of these uphill corrector steps.)

Table 11 lists the stationary points that were computed using the terrain methodology in the full space of 20 optimization variables using *two* separate starting points. One set of terrain optimizations finds the minimum B, saddle point BC, and

Table 11. Optimization Results for a Five-Element, Four-Node Spherical Catalyst Pellet Model

stationary point	minimum B	saddle BC	minimum C	local minimum G	saddle GA	minimum A
y_1	0.19403	0.74926	0.99273	7.4230×10^{-8}	1.4046×10^{-7}	-4.9433×10^{-9}
y_2	0.21203	0.74945	0.99274	4.6213×10^{-7}	8.7943×10^{-7}	-3.1188×10^{-8}
y_3	0.37773	0.75188	0.99281	-2.5068×10^{-6}	-4.7695×10^{-6}	1.6912×10^{-7}
y_4	0.44995	0.75345	0.99286	-8.7814×10^{-6}	-1.6708×10^{-5}	5.9245×10^{-7}
y_5	0.44995	0.75427	0.99286	9.2384×10^{-6}	2.8162×10^{-6}	5.9245×10^{-7}
y_6	0.57434	0.75867	0.99300	1.0082×10^{-6}	4.6185×10^{-6}	-2.9039×10^{-7}
y_7	0.77279	0.77681	0.99361	-2.7969×10^{-6}	-1.7589×10^{-5}	1.1992×10^{-6}
y_8	0.81515	0.78519	0.99393	-3.2917×10^{-5}	-2.1491×10^{-4}	1.4763×10^{-5}
y_9	0.81515	0.80095	0.99393	1.9900×10^{-4}	3.6368×10^{-5}	1.4763×10^{-5}
y_{10}	0.85376	0.81110	0.99434	-1.3226×10^{-5}	2.7032×10^{-5}	-3.4060×10^{-6}
y_{11}	0.92408	0.83869	0.99574	8.8369×10^{-5}	-1.0654×10^{-4}	1.6664×10^{-5}
y_{12}	0.94190	0.84866	0.99636	1.4541×10^{-3}	-1.7074×10^{-3}	2.7039×10^{-4}
y_{13}	0.94190	0.88291	0.99636	5.0066×10^{-3}	2.1413×10^{-3}	2.7039×10^{-4}
y_{14}	0.95048	0.88834	0.99671	-1.2032×10^{-3}	-6.5959×10^{-5}	-1.0788×10^{-4}
y_{15}	0.97078	0.90210	0.99775	1.4551×10^{-2}	2.4810×10^{-3}	9.6475×10^{-4}
y_{16}	0.97726	0.90680	0.99816	8.1759×10^{-2}	1.5053×10^{-2}	5.8205×10^{-3}
y_{17}	0.97726	0.94426	0.99816	0.19379	0.13394	5.8205×10^{-3}
y_{18}	0.98258	0.94834	0.99852	0.31423	0.21481	0.08427
y_{19}	0.99566	0.95858	0.99959	0.86597	0.83174	0.73844
y_{20}	1.00000	0.96205	1.00000	1.07207	1.07547	1.00000
F^TF	7.18×10^{-26}	0.00439	4.63×10^{-21}	0.01777	0.01985	1.70×10^{-21}
calls[a]			44 404			90 506
time[b] (s)			33.36			73.77

[a] Calls means evaluations of the function (F), gradient ($g = \mathbf{J}^TF$) and Hessian matrix ($\mathbf{H}$), where the Hessian matrix is given by $\mathbf{H} = \mathbf{J}^T\mathbf{J} + \Sigma F_i \nabla^2 F_i$. [b] Time in seconds on a Dell High Precision 670 Workstation (3.8 GHz).

minimum C. From the other starting point, the terrain method finds the local minimum G, saddle point GA, and minimum A. We note that the linear equations in the collocation model *do not* need to be (and, in fact, are not) satisfied at saddle points or local minima, where the value of F^TF is bounded away from zero. It is also important to note that solution A shown in Table 11 has some very small negative values for some of the y variables. This is largely due to the collocation procedure, which is not adaptive.

4.2. Barrier-Terrain Optimization Calculations. Here, we apply the proposed barrier-terrain methodology to this larger collocation model of the spherical catalyst pellet problem. We are interested in determining if the barrier-terrain method (i) is successful in creating a smooth connection between all physically meaningful solutions, (ii) finds all physically meaningful constrained solutions, and (iii) helps to alleviate computational difficulties that are associated with small negative dimensionless concentrations in solution A.

Remark. One important modeling aspect that aids in the solution procedure using the barrier-terrain method is to eliminate the collocation points y_5, y_9, y_{13}, and y_{17}, and boundary constraint on y_{20} by making the necessary substitutions in the remaining model equations using eqs 42−45 and eq 50, respectively. That is, we substitute the variable y_4 for y_5 in eqs 33, 34, and 46. Making similar substitutions for y_9, y_{13}, y_{17}, and y_{20} leaves 15 equations and 15 unknowns.

4.2.1. Barrier Iteration #0. We begin by selecting $\mu_0 = 10^5$. Using a random starting point, the terrain method finds a unique global minimum, $y^* = s^*(\mu_0)$, on $\phi_2(\mu_0)$, which looks qualitatively similar to solution B in Table 11. The unknown optimization variables that correspond to this unique minimum are given in Table 12, along with the corresponding value of ϕ_2, which is 2.1241×10^6. We also remark that this unique global solution persists to a barrier parameter of 10 000.

4.2.2. Barrier Problem #1. For the next barrier problem, we have selected $\mu_1 = 2500$ and use $s^*(\mu_0)$ as the starting point for the terrain optimizations. The terrain method finds a set of 22 stationary points and singular points on $\phi_2(\mu_1)$: 4 minima, 3 saddle points, and 15 singular points. We note that *all* 22 stationary and singular points were computed from one starting point—the unique minimum $y = s^*(\mu_0)$—and that this clearly establishes the necessary connection to further track stationary and singular points as μ approaches zero. Figure 9 shows augmented objective function values (ϕ_2), as a function of the barrier parameter (μ), where, for clarity, only a limited number of important stationary and singular points are shown for each value of the barrier parameter. In particular, the stationary points for $\mu = 2500$ are the rightmost set of important stationary and singular points in Figure 9 and the stationary point labeled solution B in Figure 9 is qualitatively similar to the global minimum B given in Table 11.

Table 12. Some Optimization Results for a Five-Element, Four-Node Spherical Catalyst Pellet Model

variable	minimum B ($\mu = 10^5$)	singular point A ($\mu = 25$)	minimum A ($\mu = 0.02$)	minimum B ($\mu = 0.02$)
y_1	0.48461	4.6790×10^{-4}	7.6979×10^{-5}	0.47612
y_2	0.50242	2.4869×10^{-3}	1.4218×10^{-5}	0.47932
y_3	0.50818	1.3414×10^{-2}	2.4736×10^{-4}	0.51499
y_4	0.51551	4.1131×10^{-2}	7.9474×10^{-4}	0.53531
y_5	0.51551	4.1131×10^{-2}	7.9474×10^{-4}	0.53531
y_6	0.50147	8.5965×10^{-4}	2.0822×10^{-5}	0.58173
y_7	0.50267	7.6860×10^{-3}	1.9600×10^{-4}	0.70971
y_8	0.51323	9.1751×10^{-2}	2.3988×10^{-3}	0.74832
y_9	0.51323	9.1751×10^{-2}	2.3988×10^{-3}	0.74832
y_{10}	0.50166	2.7081×10^{-3}	6.7860×10^{-5}	0.78619
y_{11}	0.50285	6.6723×10^{-3}	1.8203×10^{-4}	0.86347
y_{12}	0.51857	1.1491×10^{-1}	3.2367×10^{-3}	0.88490
y_{13}	0.51857	1.1491×10^{-1}	3.2367×10^{-3}	0.88490
y_{14}	0.49624	1.2943×10^{-2}	3.0509×10^{-4}	0.89953
y_{15}	0.48118	9.1744×10^{-2}	1.0518×10^{-3}	0.93437
y_{16}	0.48744	0.35997	6.7557×10^{-3}	0.94554
y_{17}	0.48744	0.35997	6.7557×10^{-3}	0.94554
y_{18}	0.44550	0.48715	8.4704×10^{-2}	0.95835
y_{19}	0.72860	0.86831	0.73848	0.98970
y_{20}	1.00000	1.00000	1.00000	1.00000
ϕ_2	2.1241×10^6	1.7103×10^3	2.30535	0.68372

4.2.3. Barrier Iteration #2. We set $\mu_2 = 500$ and use $s^*(\mu_1)$ to track stationary points on $\phi_2(\mu_2)$. We select solution B from the previous barrier problem to initialize the terrain calculations for this barrier iteration. Here, two local minima, two saddle points, and seven singular points on $\phi_2(\mu_2)$ were found.

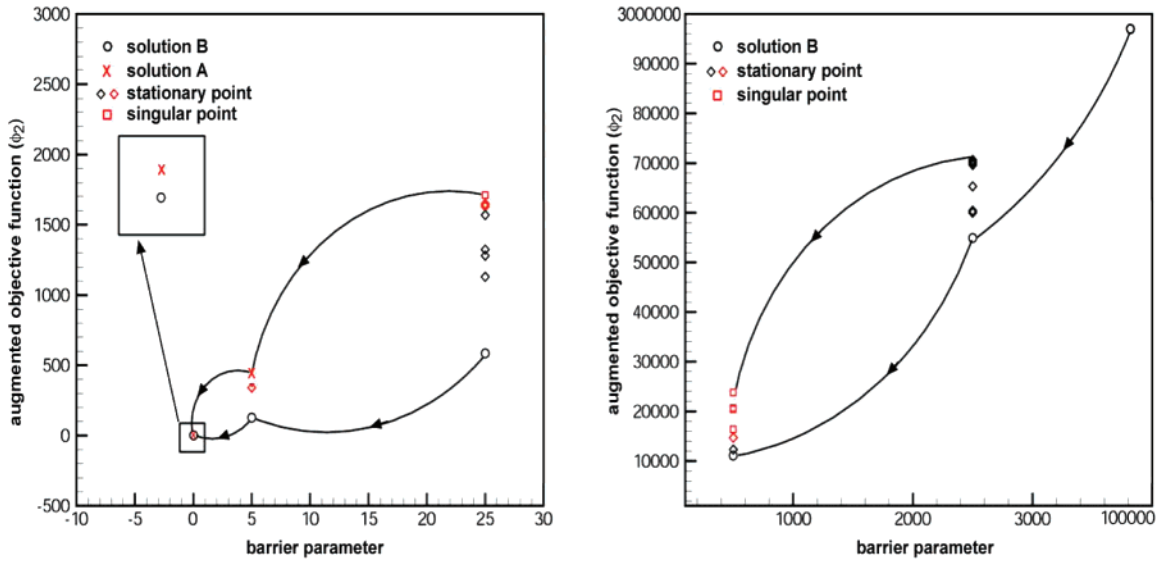

Figure 9. Stationary and singular points for a five-element, four-node catalyst pellet collocation problem.

However, it is important to note that some of the stationary points on $\phi_2(\mu_1)$ that were easily calculated in the previous barrier sub-problem proved more difficult to calculate on the surface $\phi_2(\mu_2)$ from this starting point, because of the very tightly packed level curves. On the other hand, initializing a second set of terrain calculations on $\phi_2(\mu_2)$, using the local minimum with the highest value of $\phi_2(\mu_1)$, finds nine additional stationary and singular points: two local minima, one saddle point, and six singular points. Thus, for $\mu < 500$, the path that connects all stationary and singular points is broken, two distinct valleys emerge, and, thus, two physically meaningful starting points from $s^*(\mu_1)$ must be used to find all physically meaningful points of interest on $\phi_2(\mu_2)$. Again, only those stationary and singular points of physical significance for $\mu = 500$ are shown in Figure 9.

In particular, the stationary and singular points shown in black in Figure 9 correspond to those calculated from solution B in $s^*(\mu_1)$, whereas those shown in red were calculated from the local minimum in $s^*(\mu_1)$ with the largest value of $\phi_2(\mu_1)$. We also note that this local minimum on $\phi_2(\mu_1)$ has now become a singular point on $\phi_2(\mu_2)$.

4.2.4. Barrier Iteration #3. We continue by reducing the value of μ to $\mu_3 = 25$ and use two members of $s^*(\mu_2)$ to calculate the stationary and singular points on $\phi_2(\mu_3)$. Using solution B on $\phi_2(\mu_2)$ as one of the starting points, the terrain method finds 19 stationary and singular points on $\phi_2(\mu_3)$. On the other hand, using the singular point with the largest value of $\phi_2(\mu_2)$ as the other starting point, 8 additional stationary and singular points were found. At this point, it is important to note that the *singular point* with largest value of $\phi_2(\mu_3)$, which is shown in Table 12, looks similar to the global minimum A, which has been given in Table 11.

4.2.5. Barrier Iteration #4. Here, $\mu_4 = 5$ and we select solution B and the singular point with highest value of $\phi_2(\mu_3)$ from $s^*(\mu_3)$ to track stationary and singular points on $\phi_2(\mu_4)$. From solution B in $s^*(\mu_3)$, the terrain method calculates eight stationary and singular point on $\phi_2(\mu_4)$, whereas from solution A in $s^*(\mu_3)$ or the other starting point, the terrain method finds seven stationary and singular points on $\phi_2(\mu_4)$. For this barrier iteration, the solution A that we find has changed its character from a singular point to a local minimum and looks very similar to global minimum A that has been given in Table 11—as one would expect.

4.2.6. Barrier Iteration #5. For $\mu_5 = 0.02$, we select both solution B and solution A from $s^*(\mu_4)$ to track the stationary points on $\phi_2(\mu_5)$. From solution B, the terrain method finds four stationary and singular points on $\phi_2(\mu_5)$, including one minimum that looks similar to solution B in Table 11. On the other hand, only solution A can be calculated from local minimum A in $s^*(\mu_4)$. At this barrier parameter value, solutions A and B appear very similar to minimum A and minimum B that have been given in Table 11. In particular, all of the values of the optimization variables are positive, because the barrier function forces them to be strictly positive and the value of the augmented objective function is 2.30535. Table 12 gives the values of the optimization variables and the augmented objective function for solutions A and B for $\mu = 0.02$. However, there is still no evidence of solution C.

4.3. Finalizing the Calculations. Here, we solve $F = 0$. Using solutions A and B from $s^*(\mu_5)$ to initialize the terrain methodology, all global minima given in Table 11, including solution C, are found. However, we note that solution C is extremely difficult to find using a Newton strategy. Even with a very good initial guess that comes from a perturbation of a saddle point that is very close to solution C (i.e., saddle point BC in Table 11), more than 1500 Newton iterations are still required to attain the desired accuracy.

5. Additional Information and Guidelines for Using the Barrier-Terrain Approach

Here, we provide the reader with some additional information and a list of guidelines on when to consider using the barrier-terrain approach.

5.1. Always Try the Terrain Method First. When given a new problem, our philosophy has always been to try the terrain method first without the logarithmic barrier term.

5.2. When To Use the Barrier-Terrain Approach. When the terrain approach alone is used and insufficient exploration of the feasible region occurs, then it is prudent to use the barrier-terrain approach. The numerical results shown in Figure 4 provide clear illustration of this statement. Starting at point S in the upper right-hand corner of Figure 4, it is clear that the terrain path only explores a small portion of the upper right quadrant of the feasible region. This, in our opinion, is a clear sign that the barrier-terrain method should be used to force more-thorough exploration of the feasible region.

5.3. Adjusting the Barrier Parameter. In our experience, it is best to be somewhat conservative in modifying the barrier parameter value, although not too conservative. For example, the smaller illustrative example shows that it is possible to use results for $\mu = 10^4$ to find all meaningful stationary and singular points for $\mu = 1$. However, we did not do this and, instead, used several intermediate values of μ in going from $\mu = 10^4$ to $\mu = 1$. Thus, we caution the reader. Changes in the value of the barrier parameter are problem-dependent, and this is why we recommend being somewhat conservative.

5.4. Problem Dimensionality. The proposed barrier-terrain approach is not limited by dimensionality. Although it is true that a finite-element method with five elements and four nodes is still relatively small in size, we presented this example because reporting the numerical results of stationary and singular points in tables was still tractable. We have used the terrain method to reliably solve problems with as many as 300 unknown variables. The use of an outer barrier parameter loop would not change this reliability, but it will obviously increase the computational costs.

5.5. Theoretical Guarantee of Finding All Stationary Points. A theoretical guarantee can (and, in fact, does) exist that shows that all stationary and singular points can be found. This guarantee rests on the fact that the terrain method can find *all stationary and singular points on a single path* and was proved by Lucia and Yang[22] in the absence of integral path bifurcations. The barrier approach connects valleys that are disconnected and thus creates a single path that connects all stationary and singular points. Moreover, integral path bifurcations can be reliably detected by monitoring the Gauss−Kronecker curvature, and techniques for following the relevant branches from an integral path bifurcation exist. (See the work of Lucia et al.[22]) These last two facts, coupled with the proof given in the work of Lucia and Yang,[23] provide rigorous proof that the barrier-terrain approach can find all stationary and singular points in the feasible region. However, once again, we stress that this is a theoretical proof and that, in practice, one must still address the limiting ill-conditioning difficulties that are caused by $\mu \rightarrow 0$.

5.6. Other Possible Uses of the Barrier-Terrain Approach. Although a similar framework for applying a barrier-terrain approach to mixed-integer nonlinear programming (MINLP) problems has not been considered in this work, the barrier-terrain approach could be used to solve MINLP problems, provided some important considerations were addressed. There are two possible ways in which the barrier-terrain method could be applied to MINLP problems:

(a) Use the barrier-terrain approach for only the nonlinear programming (NLP) sub-problems within an MINLP environment as structure (or integer variables) change. These integer variables could be (0, 1) variables or integer variables such as the number of stripping stages in a distillation column. Within any single NLP sub-problem in a MINLP algorithm, application of the barrier-terrain approach follows the work presented in this paper by starting with a large value of the barrier parameter and systematically reducing the value of the barrier parameter and tracking the different solutions qualitatively.

However, from one major MINLP iteration to another, in which the integer variables have changed, it is unclear if qualitatively different NLP solutions for one set of integer variables would provide a good warm start for the next set of integer variables, especially if the integer variables are (0, 1) variables and structure has appeared or disappeared.

(b) Use a superstructure and apply the barrier-terrain approach to a superstructure model. Here, there is one level of MINLP computation that contains both continuous and integer variables. Within this one-level MINLP approach, the barrier-terrain method is more promising. However, the superstructure must be complete or large enough to contain all possibilities of interest and the barrier-terrain algorithm must also be able to handle high-order singularities as integer variables appear and disappear. If high-order singularities can be handled effectively, then it is possible to move around both sub-spaces and the full space of all variables, using the barrier-terrain approach to find stationary and singular points.

6. Conclusions

A barrier-terrain methodology for global optimization was proposed where logarithmic barrier functions are used in a very unique and different manner from their purpose in previous work, in which the barrier parameter merely keeps intermediate iterates in the interior of the feasible region. In this work, we have used barrier functions in an entirely new fashion to create smooth low-lying valleys that connect all physically meaningful solutions for some set of intermediate values of the barrier parameter bounded away from zero. After a connection between all physically meaningful solutions was established, these solutions were then tracked, independently if necessary, as the barrier parameter was reduced to zero. A novel barrier-terrain algorithm was presented and applied successfully to two different collocation models for the classical reaction-transport problem in a spherical catalyst pellet originally studied by Weisz and Hicks.[15] These multiple solutions were previously identified by time-consuming shooting methods; global methods to detect all solutions of this boundary value problem robustly are not reported in the open literature. The difficulty in finding solutions to global collocation models such as those studied here is due to the very strong nonlinearity and the presence of disconnected valleys that contain different solutions. Fortunately, the barrier-terrain methodology that has been presented in this paper finds all physically meaningful solutions to these collocation models in a reliable manner. We have also presented some additional information on the expected theoretical behavior, as well as a list of guidelines for the reader, regarding how and when to use the barrier-terrain approach.

For completeness, we highlight the use of dynamic adaptive element boundaries to achieve high precision. A discussion of adaptive grid placement is beyond the scope of this paper and can be found elsewhere.[24,25]

We close by mentioning that one grand challenge for any barrier-terrain methodology is the difficulties that are associated with tightly packed level curves along the boundaries of the feasible region that occur at low barrier-parameter values. This strong ill-conditioning often makes it difficult to follow the valleys that connect solutions, and this is one aspect of the ongoing research in barrier-terrain methods.

Appendix A

The parameters γ, β, and ϕ used in eq 7 represent the dimensionless activation energy, the dimensionless heat of reaction, and the Thiele modulus as evaluated at the surface of the spherical catalyst pellet, respectively. These parameters are expressed in terms of the pellet transport and reaction properties, as well as the pellet surface concentration ($C_{A,s}$) and temperature (T_s), as follows:

dimensionless activation energy: $\gamma = \frac{E}{R_g T_s}$ (A1)

dimensionless heat of reaction: $\beta = \frac{-\Delta H D_{\epsilon z}}{K_{\epsilon z}}\left(\frac{C_{A,s}}{T_s}\right)$ (A2)

Thiele modulus: $\phi = R\left\{\frac{k_{ref}}{D_{\epsilon z}} \exp\left[\frac{-E}{R_g T_{ref}}\left(\frac{T_{ref}}{T_s} - 1\right)\right]\right\}^{1/2}$ (A3)

Acknowledgment

The authors would like to thank the reviewers for their helpful comments.

Nomenclature

C_A = concentration of reactant A inside the catalyst pellet
$C_{A,s}$ = concentration of reactant A at the surface of catalyst pellet
D_ϵ = effective diffusivity inside the catalyst pellet
E = activation energy
f = given model equations
F = reduced model equations
g = gradient of $F^T F$
$\mathbf{H}$ = Hessian matrix of $F^T F$
ΔH = heat of reaction
$\mathbf{J}$ = Jacobian matrix of F
k_{ref} = reference reaction constant
K_ϵ = effective thermal conductivity inside the catalyst pellet
l = Lagrange polynomial
L = level set value
m = number of nodes in each finite element
n = number of finite elements
OBJ = general objective function
r_A = Arrhenius reaction rate
R_g = universal gas constant
s = solution set
T = temperature inside the catalyst pellet
T_{ref} = reference temperature
T_s = temperature at the surface of catalyst pellet
V = valley
x = dimensionless radius of the spherical catalyst pellet
$x_i^{[j]}$ = ith collocation node of the jth finite element
y = dimensionless concentration along radial direction of catalyst pellet
$y_i^{[j]}$ = dimensionless concentration value ith collocation node of the jth finite element
y^L = lower bound
y^U = upper bound

Greek Symbols

β = dimensionless heat of reaction
γ = dimensionless activation energy
η = effectiveness factor
Λ = set of contours
ϕ = Thiele modulus
ϕ_2 = augmented objective function
μ = barrier parameter

Literature Cited

(1) Schnepper, C. A.; Stadtherr, M. A. Robust Process Simulation Using Interval Methods. *Comput. Chem. Eng.* **1995**, *20*, 187.
(2) Sun, A. C.; Seider, W. D. Homotopy−Continuation Algorithm for Global Optimization. In *Recent Advances in Global Optimization*; Floudas, C. A., Pardalos, P. M., Eds.; Princeton University Press: Princeton, NJ, 1992.
(3) Maranas, C. D.; Floudas, C. A. Finding All Solutions to Nonlinearly Constrained Systems of Equations. *J. Global Optim.* **1995**, *7*, 143.
(4) Kirkpatrick, S.; Gelatt, C. D.; Vecchi, M. P. Optimization by Simulated Annealing. *Science* **1983**, *220*, 671.
(5) Holland, J. H. Genetic Algorithms. *Sci. Am.* **1992**, *267*, 66.
(6) Lucia, A.; Yang, F. Multivariable Terrain Methods. *AIChE J.* **2003**, *49*, 2553.
(7) Lucia, A.; DiMaggio, P. A.; Depa, P. A Geometric Terrain Methodology for Global Optimization. *J. Global Optim.* **2004**, *29*, 297.
(8) Frisch, K. R. The Logarithmic Potential Method of Convex Programming. Memorandum, May 13, 1955, University Institute of Economics, Oslo, Norway.
(9) Fiacco, A. V.; McCormick, G. P. *Nonlinear Programming: Sequential Unconstrained Minimization Techniques*; Wiley: New York, 1968.
(10) Luenberger, D. G. *Introduction to Linear and Nonlinear Programming*; Addison−Wesley: Reading, MA, 1973.
(11) Piela, L.; Kostrowicki, J.; Scheraga, H. A. The Multiple-Minima Problem in Conformational Analysis of Molecules. Deformation of the Potential Energy Hypersurface by the Diffusion Equation Method. *J. Chem. Phys.* **1989**, *93*, 3339.
(12) Wenzel, W.; Hamacher, K. Stochastic Tunneling Approach for Global Minimization of Complex Potential Energy Landscapes. *Phys. Rev. Lett.* **1999**, *82*, 3003.
(13) Wales, D. J.; Doye, J. P. K. Global Optimization by Basin Hopping and the Lowest Energy Structures of Lennard-Jones Clusters Containing Up To 110 Atoms. *J. Phys. Chem.* **1997**, *101*, 5111.
(14) Villadsen, J. V.; Michelsen M. L. *Solution of Differential Equations by Polynomial Approximation*; Prentice Hall: New York, 1978.
(15) Weisz, P. B.; Hicks, J. S. The Behavior of Porous Catalyst Particles in View of Internal Mass and Heat Diffusion Effects. *Chem. Eng. Sci.* **1962**, *17*, 265.
(16) Fogler, H. S. *Elements of Chemical Reaction Engineering*; Prentice Hall: Upper Saddle River, NJ, 1999.
(17) Carnahan, B.; Luther, H. A.; Wilkes, J. O. *Applied Numerical Methods*; Wiley: New York, 1969.
(18) Kim, D. H.; Lee, J. A Robust Iterative Method of Computing Effectiveness Factors in Porous Catalysts. *Chem. Eng. Sci.* **2004**, *59*, 2253.
(19) Lin, Y.; Enszer, J. A.; Stadtherr, M. A. Enclosing All Solutions of Two-Point Boundary value Problems for ODEs. *Comput. Chem. Eng.* **2007**, doi:10.1016/j.compchemeng.2007.08.013.
(20) Zhang, L.; Linninger, A. A. Temperature Collocation Algorithm for Fast and Robust Distillation Design. *Ind. Eng. Chem. Res.* **2004**, *43*, 3163.
(21) Kulkarni, K. Mathematical Modeling, Problem Inversion and Design of Distributed Chemical and Biological Systems, Ph.D. Dissertation, University of Illinois at Chicago, Chicago, IL, 2007.
(22) Lucia, A.; Yang, F. Global Terrain Methods. *Comput. Chem. Eng.* **2002**, *26*, 529.
(23) Lucia, A.; DiMaggio, P. A.; Bellows, M. L.; Octavio, L. M. The Phase Behavior of *N*-Alkane Systems. *Comput. Chem. Eng.* **2005**, *29*, 2363.
(24) Cuthrell, J. E.; Biegler, L. T. On the Optimization of Differential-Algebraic Process Systems. *AIChE J.* **1987**, *33*, 1257.
(25) Tanartkit, P.; Biegler, L. T. A Nested, Simultaneous Approach for Dynamic Optimization Problems−II: The Outer Problem. *Comput. Chem. Eng.* **1997**, *21*, 1365.

Received for review October 19, 2007
Revised manuscript received January 28, 2008
Accepted January 30, 2008

IE071421T